COMMUNICATION

Mechanical rigidity of a shape-memory metal-organic framework increases by crystal downsizing

Al A. Tiba, Matthew T. Conway, Collin S. Hill, Dale C. Swenson, Leonard R. MacGillivray,* and Alexei V. Tivanski*

Received 00th January 20xx,
Accepted 00th January 20xx

DOI: 10.1039/x0xx00000x

Soft porous nanocrystals with a pronounced shape-memory effect exhibit two- to three-fold increase in elastic modulus compared to the microcrystalline counterpart as determined by atomic force microscopy nanoindentation. The increase in rigidity is consistent with the known shape-memory effect displayed by the framework solid at the nanoscale. Crystal downsizing can offer new avenues for tailoring the mechanical properties of metal-organic frameworks.

Flexible metal-organic frameworks (MOFs), or soft porous crystals (SPCs), consist of metal ions bridged by organic linkers that combine crystallinity and structural mobility to allow for large volume changes and dynamic guest adsorption properties. SPCs can exhibit cooperative structural transformability, where the pores expand from a nonporous closed phase to a highly-porous open phase in response to external stimuli (e.g. temperature, pressure, guest incorporation).[1,2] These intriguing solid-solid transitions make SPCs particularly advantageous for applications in energy storage,[3,4] chemical separations,[5] catalysis,[6] and drug delivery.[7] The mechanical properties of SPCs (e.g. elastic modulus, shear modulus, and linear compressibility) are expected to be central to their successful transition into industrial applications that require significant mechanical stress in the form of post-synthetic processing.[8]

Crystal downsizing to the nanoscale is now being used to modulate mechanical properties of porous crystalline materials.[9-16] Downsized MOFs can exhibit variable properties based on crystal size, where higher or lower applied pressures are required for efficient gas adsorption onto nanocrystals than larger bulk crystals.[10-13] Defects can also influence the mechanical properties of MOFs wherein a decrease in the number of defects leads to an increase in framework rigidity.[17] Porous and nonporous metal-organic solids exhibit size-dependent mechanical and electrical properties at the nanoscale.[18-20] In order to measure the mechanical properties of nanocrystalline materials, it is critical that chemists employ tools and/or techniques that have an inherent capacity to measure properties at the nanoscale. In this context, atomic force microscopy (AFM) nanoindentation has emerged as a tool to determine mechanical properties of nano- and macro-dimensional crystals.[16,18-23] In our work, a prototypical breathing MOF, ZIF-8, displayed a 40% reduction in elastic modulus at the nanoscale (*i.e.*, increase in flexibility).[16] Nanocrystalline MOFs are of particular relevance since properties such as porosity, flexibility, and breathing transitions can be modulated owing to cooperative interactions downsized to the molecular level.[10-13,16]

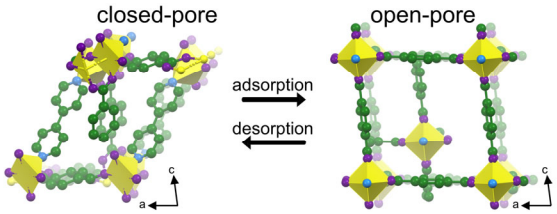

Scheme 1. Structure of $[Cu_2(bdc)_2(bpy)]_n$. Breathing transition from nonporous closed phase to porous open phase occurs as a result of methanol adsorption to give $[Cu_2(bdc)_2(bpy)]_n \supset MeOH$ (methanol guests and hydrogen atoms not shown for clarity).

Herein, we report the mechanical properties of the two-fold interpenetrated, pillared-layered SPC, $[Cu_2(bdc)_2(bpy)]_n$ (bdc = 1,4-benzenedicarboxylate, bpy = 4,4'-bipyridine).[24] The SPC is the first reported example of a very rare class of shape-memory nanoporous crystalline solids.[25] The framework exhibits a *breathing* response to sorption stress (**Scheme 1**). Shape-memory molecular frameworks retain the metastable, open-pore phase even after the release of guest molecules. The structure can be transformed back to the closed-pore phase by applying a stimulus such as temperature.[1,25,26] In that regard, crystal downsizing of $[Cu_2(bdc)_2(bpy)]_n$ to the nanoscale was reported to impart a shape-memory effect that was tentatively attributed to increased framework rigidity.[25] In contrast,

Department of Chemistry, University of Iowa, Iowa City, Iowa 52242-1294 United States

† Electronic Supplementary Information (ESI) available: Full experimental details including materials, methods, synthesis, and analysis along with characterization data from atomic force microscopy and powder X-ray diffraction. See DOI: 10.1039/x0xx00000x

no shape-memory effect was observed in microcrystals. We hypothesized that downsizing $[Cu_2(bdc)_2(bpy)]_n$ to the nanoscale likely results in stiffening of the framework that may facilitate stabilization of the open-pore phase after the release of guest molecules.[25]

Micro- and nanodimensional crystals of $[Cu_2(bdc)_2(bpy)]_n \supset MeOH$ were synthesized solvothermally (**Figs. 1a,b**, see ESI). The formations of micro- and nano-dimensional crystals of $[Cu_2(bdc)_2(bpy)]_n$ were confirmed by powder X-ray diffraction (see ESI). Microcrystals and nanocrystals in the closed phase were generated by heating the as-synthesized samples at 65 °C overnight and at 200 °C for 1 hour, respectively.[25] Conversion into the closed phase for each solid was confirmed by powder X-ray diffraction (see ESI). Monodisperse nanocrystals were achieved by a coordination modulation method using acetic acid. A modulator concentration ratio relative to copper acetate of 10 was used to minimize the average crystal size, as reported.[25] AFM imaging and nanoindentation measurements on 26 individual nanocrystals revealed crystal thicknesses of 10-30 nm and base sizes of 0.1-0.5 µm (**Fig. 1c**).

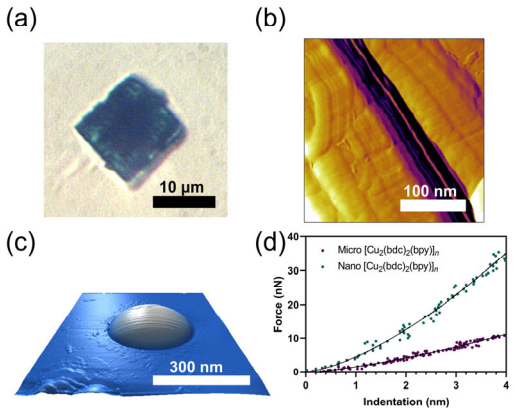

Figure 1. Imaging and AFM data for micro- and nanocrystals of $[Cu_2(bdc)_2(bpy)]_n \supset MeOH$: (a) optical microscope image of a micro-sized crystal showing plate-like square morphology, (b) AFM amplitude image of a 3 µm sized microcrystal with a smooth, layered top surface, (c) AFM 3D height image of a nanocrystal showing plate-like morphology with height of ~30 nm and base size of ~300 nm, and (d) representative force-indentation plots of the approach to the micro- and nanocrystal surfaces.

AFM nanoindentation experiments were performed using force-indentation measurements (**Fig. 2**) on micro- (blue) and nanocrystals (orange) of $[Cu_2(bdc)_2(bpy)]_n$ in the closed phase. Additional measurements were performed on micro- (purple) and nanocrystals (green) in the open phase of $[Cu_2(bdc)_2(bpy)]_n \supset MeOH$. Within the contact region of all samples, the approach and retract to the crystal surface force data were overlapping, indicative of an elastic response.[23] Detailed preparations are provided in the ESI.

Repeated force-indentation plots were collected on ten sample positions across three different microdimensional individual crystals of $[Cu_2(bdc)_2(bpy)]_n$ in the closed phase. The elastic moduli (Young's modulus) were determined by fitting each force-indentation plot to the Johnson-Kendall-Roberts (JKR) elastic contact model (see ESI).[27] Averaged elastic moduli for each microdimensional crystal were within one standard deviation, enabling values to be combined from individual crystals to a single histogram (**Fig. 2a**), yielding the most probable elastic modulus and corresponding standard deviation of E = 0.53 ± 0.11 GPa.

The open-pore phase of $[Cu_2(bdc)_2(bpy)]_n$ was generated by dispersing the microcrystals in a methanol solution. Repeated force-indentation plots were collected on eight sample positions across five different microdimensional individual crystals of $[Cu_2(bdc)_2(bpy)]_n \supset MeOH$ and the data was combined to a single histogram (**Fig. 2b**). The most probable elastic modulus and corresponding standard deviation was E = 0.33 ± 0.10 GPa.

Internal geometries of frameworks (e.g., network topology, solvent accessible volume) may influence mechanical behavior.[28] While the mechanical properties of ZIFs are mainly dependent on solvent accessible volume and topology,[29] SPCs such as $[Cu_2(bdc)_2(bpy)]_n$ may exhibit larger changes in elastic modulus as a function of guest adsorption owing to the flexible nature of the organic ligands and overall framework.[30]

Repeated force-indentation curves were collected on four individual nanocrystals in the closed phase at three to four sample positions per nanocrystal. Averaged elastic moduli for each nanocrystal were within one standard deviation and combined into a single histogram (**Fig. 2c**). The most probable elastic modulus and corresponding standard deviation was E = 1.2 ± 0.14 GPa for nanocrystals in the closed phase. The elastic modulus values of the nanocrystals are expected to represent an orientation-average response reflective of all crystallographic planes.[16,18-20]

Nanoindentation measurements were also performed on twenty two individual nanocrystals of $[Cu_2(bdc)_2(bpy)]_n \supset MeOH$ at three to four sample positions per nanocrystal. Averaged elastic moduli for each nanocrystal were within one standard deviation of each other and combined into a single histogram (**Fig. 2d**). The most probable elastic modulus and corresponding standard deviation was E = 0.98 ± 0.26 GPa for nanocrystals in the open phase. Unpaired t-tests (P < 0.02) confirmed a statistically significant difference between the elastic moduli in the two phases for micro- and nanocrystals of $[Cu_2(bdc)_2(bpy)]_n$. The elastic moduli are 20-40% higher for micro- and nanocrystals in the closed-pore phase compared to $[Cu_2(bdc)_2(bpy)]_n \supset MeOH$.

The higher elastic modulus of micro- and nanocrystalline $[Cu_2(bdc)_2(bpy)]_n$ in the closed phase is consistent with an increase in density (1.473 g/cm^3) relative to the open phase (1.240 g/cm^3).[25] Denser MOFs typically feature larger elastic moduli.[31,32] We note, instrumented nanoindentation experiments were performed on a topologically identical zinc dicarboxylate SPC, $[Zn_2(bdc)_2(dabco)]_n$ (dabco = 1,4-diazabicyclo[2.2.2]octane) or DMOF-1.[30] The mechanical properties were determined on several guest-filled phases of DMOF-1 with applied mechanical pressures comparable to AFM nanoindentation pressures used in this work (see ESI). In the current study, $[Cu_2(bdc)_2(bpy)]_n$ in the open phase is expected to be

filled with methanol guest molecules before and after AFM measurements. This is supported by the observation of similar mechanical responses as a result of repeated force measurements over the same sample position.

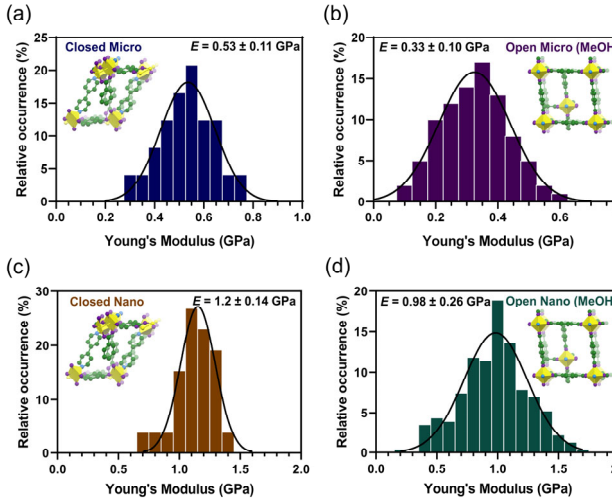

Figure 2. AFM nanoindentation data for micro- and nanocrystals of $[Cu_2(bdc)_2(bpy)]_n$: Histograms of Young's moduli for microcrystals in (a) the closed phase, (b) the methanol-filled open phase, and nanocrystals in (c) the closed and (d) methanol-filled open phase. Gaussian fits are solid black lines.

The relatively low elastic moduli or high compliance of $[Cu_2(bdc)_2(bpy)]_n$ can be attributed to the flexible nature of its framework. $[Cu_2(bdc)_2(bpy)]_n$ exhibits reversible expansion-contraction and extremely large breathing transitions with over 400 volume percent difference between the closed and open phases.[25] Atomic displacement during compression is up to several angstroms,[32] thus, the mechanical response of the framework is expected to be more compliant than non-breathing ZIFs, MOF-5, and the UiO-66 family.[16,28,29,31] The elastic moduli reported herein are lower than the elastic modulus obtained from single-crystal nanoindentation on DMOF-1 (2.1 GPa).[30] The elastic properties of $[Cu_2(bdc)_2(bpy)]_n$ are comparable to soft organic polymers, with a wide range of reported Young's moduli from 100 MPa up to several GPa.[32] Our observations for $[Cu_2(bdc)_2(bpy)]_n$ support the idea that nanoporous materials with pronounced breathing transitions may exhibit a relatively low elastic modulus.

Nanocrystals of $[Cu_2(bdc)_2(bpy)]_n$ in the closed and open-pore phases exhibited a remarkable two- to three-fold increase in elastic modulus compared to the microcrystals. Increased elastic modulus with decreasing crystal size has been observed for purely organic crystals.[18] The difference in mechanical properties at the nano- versus microscale reported here may be explained by a decrease in number of defects at the nanoscale.[17] A lower number of defects would be consistent with a framework that is stabilized in the open-pore state. At the microscale, presumably more defects and a less rigid framework provide for a more efficient single-crystal to single-crystal transformation between open and closed forms.[25,38] These observations would account for the size-dependent shape-memory adsorption effects of $[Cu_2(bdc)_2(bpy)]_n$.[25] Further studies are underway to gain insight into the possible role of defects and crystal size in other MOF systems.[33-37]

In summary, the control of crystal size and subsequent nanomechanical characterization can be valuable tools for the design of nanoporous crystals with tailored and dynamic adsorption properties. We show that the size-dependent shape-memory effect of $[Cu_2(bdc)_2(bpy)]_n$ can be ascribed to two- to three-fold increase in framework rigidity (elastic modulus) from crystal downsizing and subsequent stabilization of the metastable open-pore phase upon removal of guest molecules. Owing to dynamic breathing mechanisms of $[Cu_2(bdc)_2(bpy)]_n$ and other SPCs, the crystals belong to an emerging class of mechanical metamaterials with unique shape-shifting and topological properties.[39,40] Tuning the MOF size, defect density, and elasticity should, therefore, be desirable crystal engineering strategies to impart specific and highly unique mechanical and sorption properties.

Collin Hill acknowledges the National Science Foundation grant NSF-1757548 for the summer research experience for undergraduate (REU) program at the University of Iowa. Any opinions, findings and conclusions or recommendations expressed in this material are those of the authors and do not necessarily reflect the views of the National Science Foundation.

Conflicts of interest

There are no conflicts to declare.

Notes and references

1 M. Shivanna, Q. Y. Yang, A. Bajpai, E. Patyk-Kazmierczak and M. J. Zaworotko, *Nat. Commun.*, 2018, **9**, 3080.
2 D. Tanaka, K. Nakagawa, M. Higuchi, S. Horike, Y. Kubota, T. C. Kobayashi, M. Takata and S. Kitagawa, *Angew. Chem. Int. Ed.*, 2008, **47**, 3914-3918.
3 B. Li, H. M. Wen, W. Zhou and B. Chen, *J. Phys. Chem. Lett.*, 2014, **5**, 3468–3479.
4 R. E. Morris and P. S. Wheatley, *Angew. Chem. Int. Ed.*, 2008, **47**, 4966-4981.
5 S. Qiu, M. Xue and G. Zhu, *Chem. Soc. Rev.*, 2014, **43**, 6116–6140.
6 J. Lee, O. K. Farha, J. Roberts, K. A. Scheidt, S. T. Nguyen and J. T. Hupp, *Chem. Soc. Rev.*, 2009, **38**, 1450–1459.
7 M. X. Wu and Y. W. Yang, *Adv. Mater.*, 2017, **29**, 1606134.
8 S. Hindocha and S. Poulston, *Faraday Discuss.*, 2017, **201**, 113–125.
9 X. Yang, H. L. Zhou, C. T. He, Z. W. Mo, J. W. Ye, X. M. Chen and J. P. Zhang. *Research*, 2019, 9463719.
10 S. Krause, V. Bon, H. Du, R. E. Dunin-Borkowski, U. Stoeck, I. Senkovska and S. Kaskel, *Beilstein J. Nanotech.*, 2019, **10**, 1737-1744.
11 S. Krause, V. Bon, I. Senkovska, D. M. Többens, D. Wallacher, R. S. Pillai, G. Maurin and S. Kaskel, *Nat. Commun.*, 2018, **9**, 1573.
12 S. Tanaka, K. Fujita, Y. Miyake, M. Miyamoto, Y. Hasegawa, T. Makino, S. Van der Perre, J. C. Saint Remi, T. Van Assche, G. V. Baron and J. F. M. Denayer, *J. Phys. Chem. C.*, 2015, **119**, 28430-28349.
13 C. Zhang, J. A. Gee, D. S. Sholl and R. P. Lively, *J. Phys. Chem C.*, 2014, **118**, 20727-20733.

14 C. R. Marshall, S. A. Staudhammer and C. K. Brozek, *Chem. Sci.*, 2019, **10**, 9396-9408.
15 B. Liu, K. Vellingiri, S. H. Jo, P. Kumar, Y. Sik Ok and K. H. Kim, *Nano Res.*, 2018, **11**, 4441-4467.
16 A. A. Tiba, A. V. Tivanski and L. R. MacGillivray, *Nano Lett.*, 2019, **19**, 6140-6143.
17 T. D. Bennett, A. C. Cheetham, A. H. Fuchs and F. X. Coudert, *Nat. Chem*, 2017, **9**, 11-16.
18 C. Karunatilaka, D. K. Bučar, L. R. Ditzler, T. Friscic, D. C. Swenson, L. R. MacGillivray and A. V. Tivanski, *Angew. Chem. Int. Ed.*, 2011, **50**, 8642-8646.
19 T. P. Rupasinghe, K. M. Hutchins, B. S. Bandaranayake, S. Ghorai, C. Karunatilake, D. K. Bučar, D. C. Swenson, M. A. Arnold, L. R. MacGillivray and A. V. Tivanski, *J. Am. Chem. Soc.*, 2015, **137**, 12768-12771.
20 K. M. Hutchins, T. P. Rupasinghe, S. M. Oburn, K. K. Ray, A. V. Tivanski and L. R. MacGillivray, *CrystEngComm*, 2019, **21**, 2049.
21 Z. Zeng and J. C. Tan, *ACS Appl. Mater. Interfaces*, 2017, **9**, 39839-39854.
22 Y. Sun, Z. Hu, D. Zhao and K. Zeng, *ACS Appl. Mater. Interfaces*, 2017, **9**, 32202-32210.
23 T. I. Lansakara, F. Tong, C. J. Bardeen and A. V. Tivanski, *Nano Lett.*, 2020, **9**, 6744-6749.
24 K. Seki, *Phys. Chem. Chem. Phys.*, 2002, **4**, 1968-1971.
25 Y. Sakata, S. Furukawa, M. Kondo, K. Hirai, N. Horike, Y. Takashima, H. Uehara, N. Louvain, M. Meilikhov, T. Tsuruoka, S. Isoda, W. Kosaka, O. Sakata and S. Kitagawa, *Science*, 2013, **339**, 193-196.
26 M. Shivanna, Q. Y. Yang, A. Bajpai, S. Sen, N. Hosono, S. Kusaka, T. Pham, K. A. Forrest, B. Space, S. Kitagawa and M. J. Zaworotko, *Sci. Adv.*, 2018, **4**, eaaq1636.
27 K. L. Johnson, K. Kendall, A. D. Roberts and D. Tabor, *Proc. R. Soc. London, Ser. A*, 1971, **324** (1558), 301-313.
28 J. C. Tan and A. K. Cheetham, *Chem. Soc. Rev.*, 2011, **40**, 1059-1080.
29 J. C. Tan, T. D. Bennett and A. K. Cheetham, *Proc. Natl. Acad. Sci. U. S. A.*, 2010, **107**, 9938-9943.
30 S. Henke, W. Li and A. K. Cheetham, *Chem. Sci.*, 2014, **5**, 2392-2397.
31 H. Wu, T. Yildirim and W. Zhou, *J. Phys. Chem. Lett.*, 2013, **4**, 925-930.
32 A. U. Ortiz, A. Boutin, A. H. Fuchs and F. X. Coudert, *Phys. Rev. Lett.*, 2012, **109**, 195502.
33 L. Lingmei, Z. Chen, J. Wang, D. Zhang, Y. Zhu, S. Ling, K. W. Huang, Y. Belmabkhout, K. Adil, Y. Zhang, B. Slater, M. Eddaoudi and Y. Han, *Nat. Chem*, 2019, **11**, 622-628.
34 K. Y. Cho, J. Y. Seo, H. J. Kim, S. J. Pai, X. H. Do, H. G. Yoon, S. S. Hwang, S. S. Han and K. Y. Baek, *Appl. Catal. B-Environ.*, 2019, **245**, 635-647.
35 S. Wang, Z. W. Wei, J. Zhang, L. Jiang, D. Liu, J. J. Jiang, R. Si and C. Y. Su, *IUCrJ*, 2019, **6**, 85-95.
36 J. Hou, P. D. Sutrisna, T. Wang, S. Gao, Q. Li, C. Zhou, S. Sun, H. C. Yang, F. Wei, M. T. Ruggiero, J. A. Zeitler, A. K. Cheetham, K. Liang and V. Chen, *ACS Appl. Mater. Interfaces*, 2019, **11**, 5570-5577.
37 R. Zhang, D. Zhang, Y. Yao, Q. Zhang, Y. Xu, Y. Wu, H. Yu and G. Lu, *ACS Appl. Mater. Interfaces*, 2019, **11**, 21010-21017.
38 I. W. Chen and Y. H. Chiao, *Acta. Mater.*, 1985, **33**, 1827-1845.
39 K. Bertoldi, V. Vitelli, J. Christensen and M. van Hecke, *Nat. Rev. Mater.*, 2017, **2**, 17066.
40 F. X. Coudert and J. D. Evans, *Coord. Chem. Rev.*, 2019, **388**, 48-62.

Table of Contents Graphic:

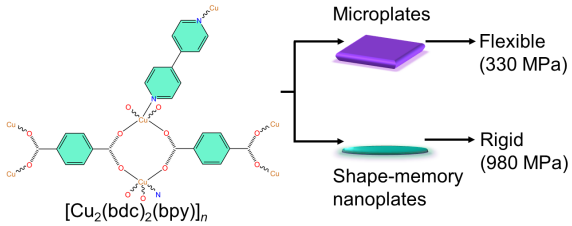

The elastic modulus of a flexible metal-organic framework increases at the nanoscale as measured using AFM nanoindentation and accounts for a known shape-memory effect.